Geophysical Journal International

Geophys. J. Int. (2015) **203,** 79–91 doi: 10.1093/gji/ggv283
GJI Marine geosciences and applied geophysics

Geoelectrical characterization of carbonate and silicate porous media in the presence of supercritical CO_2–water flow

Luqman Kolawole Abidoye and Diganta Bhusan Das

*Chemical Engineering Department, Loughborough University, Loughborough, Leicestershire, LE*11 3*TU, United Kingdom. E-mail: D.B.Das@lboro.ac.uk*

Accepted 2015 June 30. Received 2015 June 29; in original form 2014 July 7

SUMMARY

The relative permittivity (ε_r) and the electrical conductivity (σ) of porous media are known to be functions of water saturation (S). As such, their measurements can be useful in effective characterisations and monitoring of geological carbon sequestration using geoelectrical measurement techniques. In this work, the effects of pressure, temperature and salt concentration on bulk ε_r–S and σ–S relationships were investigated for carbonate (limestone) and silicate porous media (both unconsolidated domains) under dynamic and quasi-static supercritical CO_2 ($scCO_2$)-brine/water flow. In the silica sand sample, the bulk ε_r (ε_b) for $scCO_2$–water decreases as the temperature increases. On the contrary, slight increase was seen in the ε_b with temperature in the carbonate sample for the $scCO_2$-water system. These trends are more conspicuous at high water saturation. The ε_b–S curves for the $scCO_2$–water flow in the silica sand also show clear dependency on the domain pressure, where ε_b increases as the domain pressure increases. Furthermore, the bulk σ (σ_b), at any particular saturation for the $scCO_2$-brine system rises as the temperature increases with more significant increase found at very high water saturation. Both ε_b and σ_b values are found to be greater in the limestone than silica sand porous samples for similar porosity values. Based on different injection rates investigated, we do not find significant dynamic effects in the ε_b–S and σ_b–S relationships for the $scCO_2$-brine/water system. As such, geoelectrical characteristics can be taken as reliable in the monitoring of two-phase flow system in the porous media. It can be inferred from the results that the geoelectrical techniques are highly dependent on water saturation. This dependence is more conspicuous at higher water saturation. Different mathematical models examined show their reliability at different water saturation ranges. The polynomial fit developed in this work takes into consideration the fluid pressure in the system as well as the initial bulk relative permittivity prior to the injection of CO_2. The polynomial fit shows a good reliability in the prediction of the geo-electrical properties of the CO_2–water–porous media system, especially at higher water saturation. In comparison, the mixing model from the literature shows more reliability in the prediction of similar property at lower water saturation.

Key words: Electrical properties; Hydrology; Permeability and porosity; High-pressure behaviour.

1 INTRODUCTION

The issue of global warming and the possibility of geological carbon sequestration have increased the interests on studying supercritical CO_2 ($scCO_2$) and brine/water flow in porous medium (Benson & Cole 2008; Khudaida & Das 2014; Abidoye *et al.* 2015). Logically, a carbon sequestration operation in an aquifer should be safe guarded from CO_2 leakage into the atmosphere and/or CO_2 migration into potable water aquifer that might lie above a sequestration aquifer (Dethlefsen *et al.* 2013). Thus, the efficient operation of CO_2 sequestration activities and effective monitoring are keys to the success/safety of the overall process. Effective monitoring of geological carbon sequestration requires not only prior understanding of any adverse effects of different aspects of the operations but also the *in situ* mechanisms in the subsurface that may affect the sequestration process. In this regard, one needs the understanding of the constitutive relationships that govern immiscible flow in porous media, namely, the capillary pressure-saturation and relative permeability relationships (P^c–S–K_r) (see e.g. Doughty 2007; Aggelopoulos & Tsakiroglou 2008; Khudaida & Das 2014) and/or geoelectrical characteristics of the system (see e.g. Nakatsuka *et al.* 2010; Abidoye *et al.* 2015).

Interestingly, the capillary pressure (P^c), relative permeability (K_r) and electrical properties of a two-phase flow system in porous

media are functions of water saturation (see e.g. Plug *et al.* 2007). There are two principal electrical properties, namely, (i) the relative permittivity (ε_r), which is a measure of the electrical polarization of the material (Mahmood *et al.* 2012) that takes place when an electric field is applied and (ii) the electrical conductivity (σ), which is a measure of the conduction current resulted from an electric field through the material (see e.g. Keller 1966; Solymar *et al.* 2014). These properties can provide valuable information about the macro- and microscopic properties of geological formations. For example, understanding of the electrical parameters have shown good promises in the subsurface characterization activities at sites contaminated with dense non-aqueous phase liquids (DNAPLs; Archie 1942; Schmutz *et al.* 2012; Power *et al.* 2013). The applications of geoelectrical techniques in two-phase flow systems and the interpretations of the resultant information depend on the knowledge of the relationships between the effective electrical parameters and the petrophysical relationships of the constituent parts of the porous domain (i.e. solid minerals and interstitial fluid) (Ellis *et al.* 2010). These parameters are mainly utilised based on the advantages of their sensitivities to change in the saturation of the aqueous phase. As such, the geoelectrical techniques have been proposed in research and industries for monitoring the behaviours of two-phase flow systems. These techniques are useful in monitoring strong contrasts in electrical resistivity when the aquifer brine is replaced with compressed gas (Dethlefsen *et al.* 2013). Since preferential pathways may exist in the subsurface for the upward migration of CO_2 while contaminating near surface aquifers, the use of these techniques should be developed prior to the commencement of the sequestration processes. Thus, geoelectric techniques can be successfully applied in the characterization and monitoring of the $scCO_2$–water flow system.

However, one of challenges in the two-phase flow characterization (i.e. P^c–S–K_r functions) include their non-unique behaviour as the flow seems to vary with a number of parameters (Abidoye *et al.* 2015). Factors found to contribute to the non-uniqueness of the P^c–S–K_r functions in two-phase flow systems in porous media have been reported to also affect the geoelectrical properties and saturation relationships in such systems (Doussan & Ruy 2009). For example, hysteresis is reported for P^c–S relationships depending on phase distribution, saturation history ascribed to contact angle hysteresis, irreversible changes in pore-scale fluid distribution and the interfacial area (Plug *et al.* 2007; Mirzaei & Das 2013). The electrical characteristics of the two-phase flow system also exhibit hysteresis, for example, the electrical resistivity curve of two-phase flow system is higher under drainage than imbibition (Longeron *et al.* 1989; Knight 1991; Knight & Abad 1995; Verwer *et al.* 2011). This invariably translates to similar phenomenon but with the opposite effect on electrical conductivity as it is the reciprocal of the electrical resistivity. Nguyen *et al.* (1999) reported the same effect for complex relative permittivity though it is partly higher for imbibition at saturation ($S > 0.6$) and vice versa at lower saturation values.

In the same vein, water content and temperature of the fluid-fluid-porous media system are some of the factors which affect the bulk relative permittivity–saturation relationship (ε_b–S) as well as the bulk electrical conductivity–saturation relationship (σ_b–S) in the porous media. Plug *et al.* (2007) and Drnevich *et al.* (2001) showed that the bulk relative permittivity (ε_b) of an unconsolidated porous medium increases with the increase in water saturation. This can be attributed to the high value of ε_r for water over the sand medium. Thus, as the water saturation decreases, ε_b decreases. Similarly, Knight & Nur (1987) have found that the dielectric response of a porous domain is dependent on the layer of water formed around the grains which make the media. As such, water-wet media samples should have higher ε_b under flow conditions. Also, temperature is reported to influence the value of ε_b in a number of ways. The relative permittivity of water (ε_w) decreases significantly with increase in temperature (Roth *et al.* 1990) but that of most solids seem independent of temperature (Drnevich *et al.* 2001). Accordingly, the ε_b for fluid-media system will be affected by the influence of temperature which will be directly related to the amount of water present in the sample. The work of Knight & Nur (1987) can be related to the findings of Wraith & Or (1999) on the influence of bound and free water in different soil types. It has been shown that while ε_b decreases with temperature, it increases with the release of bound water at high temperature. This is the case with the medium, which has a tendency to retain high amount of bound water, for example, clay. Drnevich *et al.* (2001) show these phenomena with temperature effects using consolidated (cohesive) and unconsolidated (non-cohesive) soils. While relative permittivity increases with temperature in consolidated soil system, for example, water and clay, the opposite trend is found in unconsolidated soil system such as sand saturated with water. Relative permittivity (ε_r) is defined as follows:

$$\varepsilon_r = \varepsilon/\varepsilon_o \tag{1}$$

where ε is the dielectric permittivity (in F m^{-1}) and, ε_o is dielectric permittivity of the vacuum which has a value of 8.854×10^{-12} F m^{-1}.

Also, the bulk electrical conductivity, σ_b, was reported to increase with increase in temperature (Wraith & Or 1999). This was explained to be due to increased electrical conductivity of the materials together with elevated mobility of ions, at higher temperatures (Revil *et al.* 1998). The electrical conductivity is particularly important in $scCO_2$–water system as sequestration is mostly performed in aquifer of high salinity (Lagneau *et al.* 2005). Since CO_2 is a resistive gas (Breen *et al.* 2012), it will definitely have reverse effect on the σ_b–S relationship $scCO_2$-brine system in the porous medium. Breen *et al.* (2012) showed the application of the electrical resistivity technique in the monitoring of $scCO_2$ injection, volume and spatial distribution in quartz sand. Also, Plug *et al.* (2007) showed a work on the dielectric properties of CO_2–water system using novel method of parallel—plate capacitor which doubles as the porous medium sample holder. However, the measurements were made at below the supercritical conditions of CO_2.

The above discussions show the strong dependency of the electrical parameters on the wetting phase saturation, media characteristics, temperature and other factors. Concerning geoelectrical characterization of $scCO_2$-brine/water system, one can readily observe that the existing works are far from being exhaustive. Most of the works reported so far are related to water–sand system primarily under ambient conditions. The few works on CO_2-brine/water system that have been reported are concerned with either single phase flow in porous medium (Breen *et al.* 2012) or subcritical condition for CO_2 (Plug *et al.* 2007).

Geological sequestration of $scCO_2$ often takes place in silicate and carbonate aquifers. So an important question arises, that is, how do the geoelectrical characteristics of the $scCO_2$-brine/water system depend on these media? Also, the desaturation rate has been shown to affect the P^c–S–K_r relationships in oil/gas–water flow systems in porous media (see e.g. Kalaydjian 1992; Hassanizadeh *et al.* 2002; Das *et al.* 2007). Similar behaviour has been numerically investigated and reported for $scCO_2$-brine/water system (Das *et al.* 2014; Khudaida & Das 2014). Therefore, one can ask

for the experimental investigation of the impact of the desaturation rate on the ε_b–S and σ_b–S relationships for $scCO_2$-brine/water system. To address these questions, this work aims to comprehensively investigate the effects of the media characteristics, temperature and pressure as well as salinity on the geoelectrical characteristics of the $scCO_2$–water system in the silicate and carbonate unconsolidated porous media using a technique of time domain reflectometry (TDR) method. Furthermore, the effect of desaturation rate will be systematically investigated in repetitive experiments. The principle and the techniques of the TDR applications are explained in the methodology.

2 MATERIALS AND METHODS

2.1 Unconsolidated porous materials

The porous media used in this work were silica sand, referred to as DA 14/25 and limestone, referred to as Trucal 6. DA 14/25 and Trucal 6 were obtained from Minerals Marketing Company (Cheshire, UK) and the Tarmac Buxton Lime and Cement (Buxton, UK), respectively. Physical and chemical properties of the samples are listed in Table 1. The table shows that the physical properties of the two porous media are very similar. Before use, they were pretreated by washing in deionised water and dried for at least 24 hr to remove any clay content. To ensure uniform deposition in every experimental run, the sand was poured through a large sieve into the cell, which initially contains water to minimize air trap. The size of the domain utilized in this experiment was 4 cm height by 10.2 cm diameter.

2.2 Instrumentations and sample holder set up

In situ bulk relative permittivity and electrical conductivity measurements were made with the help of three-pin time domain reflectometry probes (TDR probes). The pins were locally constructed and held together with high temperature PTFE base holder to be used under high pressure and high temperature conditions. The rods were insulated in the region of contact with the steel cell to avoid interference with the signal. The TDR probes cable was connected to a multiplexer, which was attached to TDR100 reflectometer (Campbell Scientific Ltd, Shepshed, UK). This was then connected to CR10X datalogger (Campbell Scientific Ltd). 12 V and 50 Hz dual rail power supply (Rapid Electronics Ltd, Essex, UK) was used to supply power to the CR10X datalogger (Campbell Scientific Ltd) which was connected to the computer for automatic logging of data collected from the TDR probes inserted into the porous medium. At the start of the experiment, the TDR probes were calibrated to get the offset and multiplier following the Campbell Scientific Instruction manual. The readings were used in developing the program used in communicating the TDR100 to the datalogger. The TDR100 has a timing resolution of 12.2 picoseconds for two-way travel and the pulse length of 14 μs.

Table 1. Material properties.

Sample	$CaCO_3$ particles (Trucal 6)	SiO_2 particles (DA14/25)
Permeability, K (m^2)	4.53×10^{-10}	3.65×10^{-10}
Porosity, ϕ (–)	0.39	0.37
Particle density (g cm^{-3})	2.69	2.74
Average particle diameter, D_p (μm)	1200	946.1
SiO_2 (per cent)	–	99[a]
$CaCO_3$ content (per cent)	>98[b]	–

[a] www.sibelco.co.uk (accessed May 2014).
[b] www.lafargetarmac.com (accessed May 2014).

Fig. 1 is a schematic diagram of the experimental set up. The figure illustrates the domain size as well as the TDR probes at the centre of the sample holder. Pressure transducers (PTs) are included at the centre of domain to measure the *in situ* system pressure for different experiments. Detail description of the PTs configuration is not included in this work. The sample holder was situated in a heating cabinet. To maintain predetermined temperature in the system, electric heaters were placed at the corners of the heating cabinet while the system temperature was regulated using PID temperature controller (West Control Solutions, Brighton, UK). The set temperature was left overnight to ensure equilibration. The sample holder is a 4 cm high stainless steel cell with 10 cm diameter having stainless steel end-pieces at the top and bottom. Narrow steel tubes run upstream and downstream of the cell with inlet for $scCO_2$ (at top) and outlet for water (at the bottom). The inner parts of the top and bottom end pieces are overlaid with hydrophobic polytetrafluoroethylene, PTFE (0.1 μm) and hydrophilic nylon (1 μm), respectively. The membranes were purchased from Porvair Filtration Group Ltd (Hampshire, UK). It was reported that hydrophilic membrane minimises $scCO_2$ escape from the bottom of the sample holder (Plug & Bruining 2007) while hydrophobic membrane was used to prevent excursion of water out of the top of the sample holder into the $scCO_2$ pump. Distributor was used above the hydrophobic membrane to ensure even infiltration of the $scCO_2$. For fine control of outflow, metering valve (Swagelok, Kings Langley, UK) was located at the exit of the sample holder. Following the metering valve was the precision back pressure regulator (BPR) (Equilibar, Fletcher, USA) that kept the system and outflow at the set pressure. The back pressure regulator was a dome loaded type using PTFE-glass diaphragm and was loaded with nitrogen gas from a nitrogen cylinder (BOC gases, Leicester, UK) controlled with a single stage regulator.

2.3 Experimental procedure

2.3.1 Equipment set up

All experiments were conducted in a 4 cm sample holder cell (Fig. 2). At the start of the experiment, the equipment was set up from bottom upward. After placing the sample holder on the bottom end piece with overlaying of the hydrophilic membrane, small amount of water was poured into the cell to a certain position followed by pouring of sand through a metal sieve of appropriate size to ensure uniform sand deposition and prevent air trap. Equal amount of sand (500 g) was used in all cases. Then, the top end piece with the hydrophobic membrane was put in position. After tightening all the joint bolts, deionised water or brine was passed into the sample from tank and pressurised up to the experimental set pressure using hand pump. At this pressure, all air present in the tubing and sand was considered dissolved (Plug & Bruining 2007). Water tank valve (V6) was then closed. CO_2 used in this work was obtained from BOC gases (Leicester, UK) at 99.9 per cent purity. The supercritical fluid pump (Teledyne Isco, Lincoln NE) was filled with liquid CO_2 from the CO_2 cylinder by opening of the valve 1 and setting the pump on refill mode. Then the cylinder valve 1 was closed and the supercritical fluid pump was set at the experimental pressure. This supplied the liquid CO_2 to the tubing from the exit of the supercritical fluid pump up to the valve 3 (Fig. 1) which serves

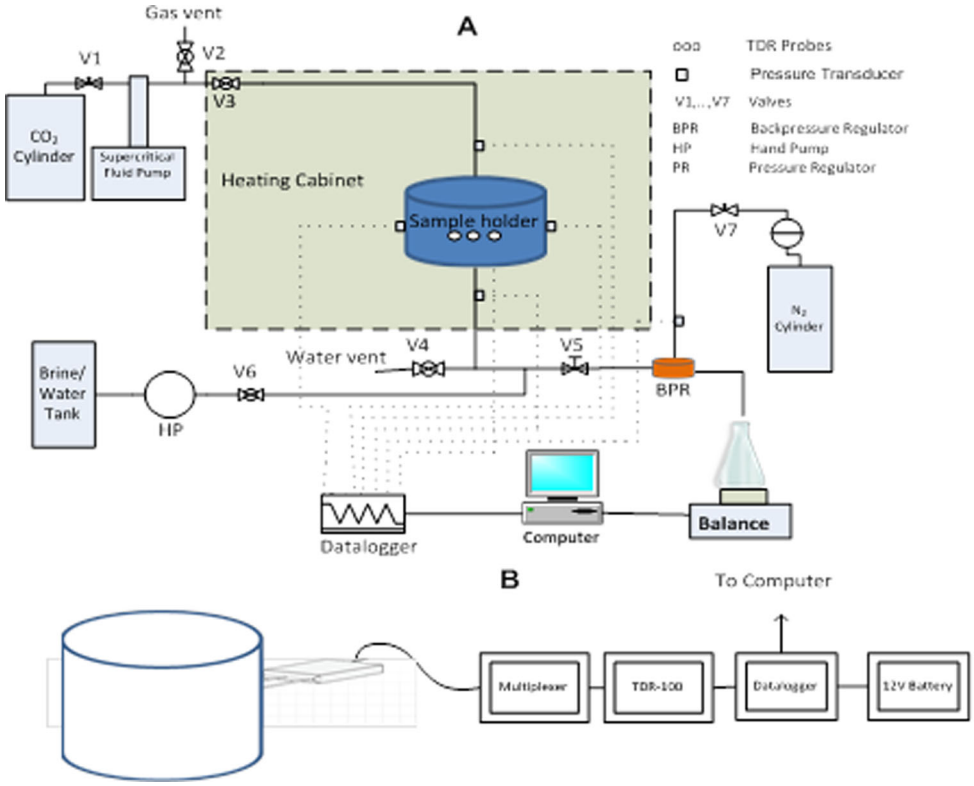

Figure 1. (a) High-pressure experimental set-up for the $scCO_2$-water system. (b) Schematics of TDR measurement system.

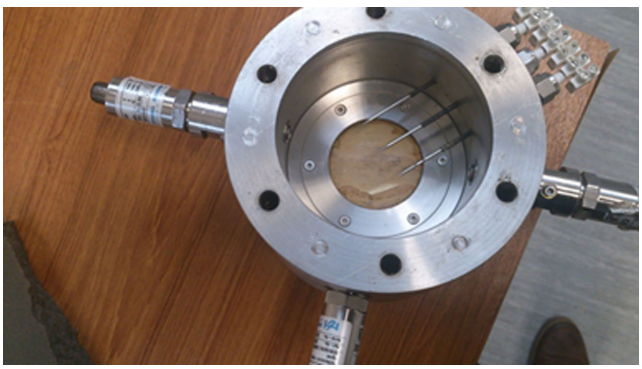

Figure 2. A photograph of the sample holder showing the TDR probes with insulation (cell internal diameter: 10 cm, sample height: 4 cm).

as the interface between water and CO_2. When the $scCO_2$ pump is set at the experimental condition, the heater is switched on and set at the experimental temperature. When the experimental conditions (temperature and pressure) reached equilibrium, V3 and V5 are opened and the displacement of brine/water began by $scCO_2$. At the end of each experiment, the porous media sample was vacuumed and washed by passage of several volumes of deionised water. Details of the experimental procedure under dynamic and quasi-static conditions are explained below.

2.3.2 Dynamic and quasi static drainage experiments

For the dynamic drainage, the backpressure regulator (BPR) was set at a constant pressure as monitored on the regulator situated on the nitrogen cylinder as well as the pressure transducer installed on the nitrogen cylinder line close to the BPR. The supercritical fluid pump was set at constant flow rate mode at a minimum rate of 5 ml min^{-1} for the dynamic drainage. This corresponds to about 2.3 pore volume per hour (PV hr^{-1}). For the quasi-static drainage, constant flow rate was set at 0.1 ml min^{-1} corresponding to about 0.05 PV hr^{-1}. Plug & Bruining (2007) used range of injection rates between 0.01 and 0.1 PV hr^{-1} to demonstrate quasi-static displacement of water by $scCO_2$ in porous media. Therefore, judging from our injection rate (0.05 PV hr^{-1}), the displacement in this work can be taken as sufficiently quasi static. The objective of this was to find the effect of desaturation rate on the bulk properties considered (relative permittivity and electrical conductivity). Drainage or displacement of brine/water continued till there was no appreciable change in the amount of brine/water collected in the outflow bottle placed on the accurate weighing balance. The weighing balance (AandD Engineering, San Jose, USA) was also connected to the computer to log the collected data in sync with the data obtained from CR10X datalogger. Some experiments were repeated two or three times to allow for statistical analysis. Measurements were performed at different temperatures (20, 40 and 50 °C) as well as different pressures (20 and 80 bar). Much noise appeared in the data from the bulk relative permittivity measurements and were smoothened using 'rloess' function in MATLAB. The function carries out a regression of the reference data by using a combined weighted linear least square and second-degree polynomial model. It assigns lower weight to outliers in the regression.

2.3.3 Bulk relative permittivity (ε_b) and electric conductivity (σ_b) measurements

The TDR probes used in this work were calibrated to obtain the probe offset and electrical conductivity constant (K_p) as instructed

Table 2. The electrical conductivity of the water used in the experiments (values taken at room temperature).

Salt (NaCl) content (g l^{-1})	Electrical conductivity (σ) (S m^{-1})
0	2×10^{-3}
10	1.4
50	5.7

in the manual (Campbell Scientific Ltd, Shepshed, UK) and were then inserted into the sample holder. They served as the waveguide extension on the coaxial cable connected to the TDR100. The TDR100 generates the electrical impulses, which travel through the coaxial cable connected to the TDR probes. Owing to contrast in impedance resulting from materials surrounding the TDR probes, reflection occur which is sent back to the source (TD100). TDR100 samples and digitizes the reflection waveforms to infer the impedance value. The impedance value is related to the geometrical configuration of the probe and inversely related to the relative permittivity of the surrounding medium. Complex permittivity (ε^*) of a material indicates the extent to which the charge distribution within a material is polarised under the influence of external electric field. Polar molecules such as water became polarised in the presence of the applied electric field owing to the absorbed energy by its molecules. The real (energy storage) and the imaginary (ionic conduction) parts (Robinson *et al.* 1999) constitute the impedance which can be used in characterising the fluid–fluid–media system. Owing to sharp contrast between the relative permittivity of the porous medium and the surrounding fluids, a change in fluid content causes a change in the bulk relative permittivity, which is seen as a change in probe impedance affecting the shape of the reflected waveform. Information from the differences in shape of the reflection is used by the TDR measurement system to determine the relative permittivity and the electrical conductivity. Since the presence of high amount of salt in the medium causes attenuation of the signal at the probe, the experiments in this work did not perform simultaneous measurements of both ε_b and σ_b. Instead, separate experiments with 1, 5 and 10 per cent reagent grade sodium chloride (Fisher Scientific, Loughborough, UK) were performed to determine σ_b for the $scCO_2$-water system. The electrical conductivity of the water used in the experiments are shown in Table 2.

3 RESULTS AND DISCUSSIONS

3.1 Relative permittivity

The effective monitoring of $scCO_2$-water flow in the subsurface will depend on the adequate characterization of the $scCO_2$-brine/water and porous media system. Since different aquifers will likely exist at different conditions, the effects of the prevalent conditions on the geoelectrical characteristics of the $scCO_2$-brine/water-porous media system will go a long way to determine reliability of the monitoring process. Here, we discuss the results of various factors investigated in connection with the σ_b–S and ε_b–S relationships for $scCO_2$-brine/water-porous media systems. As reproducibility of the measurements is important, Fig. 3 is included in this paper which demonstrates that the results of this work are reproducible. The figure shows two separate measurements (A and B) for ε_b–S relationships under the similar conditions. One can observe that the two runs (A and B) for ε_b–S curves are essentially similar in values and patterns. Similar reproducibility in results is found for the σ_b–S relationship (not shown). The figure further shows that the ε_b is a strong function of water saturation and it decreases as the water saturation reduces.

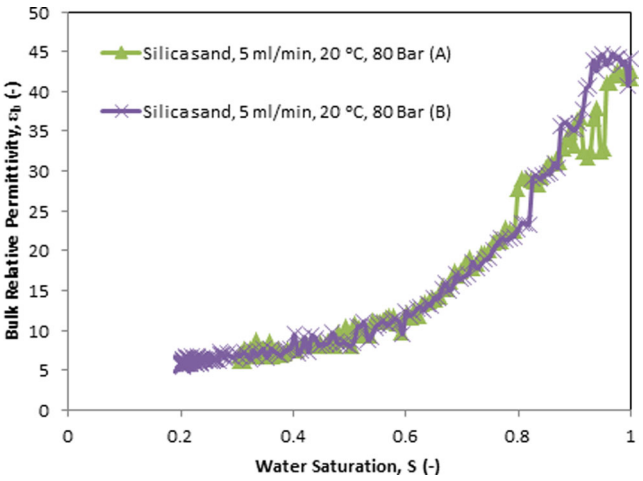

Figure 3. Reproducibility plot of ε_b–S relationship for CO_2–water–silica sand system.

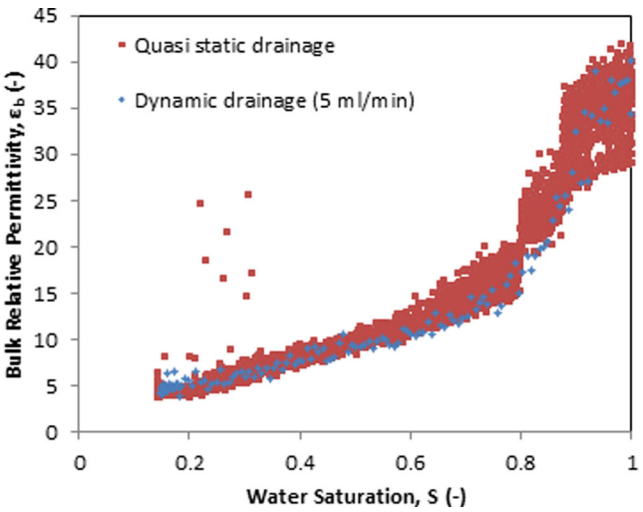

Figure 4. Drainage under quasi static and faster injection rate (5 ml min^{-1}) in $scCO_2$–water–silica sand system at 80 bar and 40 °C.

Effects of desaturation rate on the measured bulk relative permittivities and bulk electrical conductivity during the drainage process were determined. This is related to the 'dynamic effect' widely reported in the P^c–S relationships for many two-phase flow systems (Kalaydjian 1992; Hassanizadeh *et al.* 2002; Camps-Roach *et al.* 2010; Goel & O'Carroll 2011; Hou *et al.* 2012; Das & Mirzaei 2013). It refers to the dependence of the system properties on the desaturation rate in the medium (Das *et al.* 2007; Hou *et al.* 2012). Our findings do not show significant dynamic effects in the ε_b–S and σ_b–S relationships. Fig. 4 displayed this fact for the ε_b–S relationships, respectively. In Fig. 4, the data from quasi static displacement appeared dense because the drainage takes place over 24 hr with data collected every 10 s while the drainage under faster injection rate (5 ml min^{-1}) takes place in less than 2 hr at the same data collection rate. It could be seen that the data from both drainage conditions overlaid each other for most part of the water saturation with the exception of much noise in the data from quasi-static drainage. Similar results are found for the σ_b–S relationship which we discuss later.

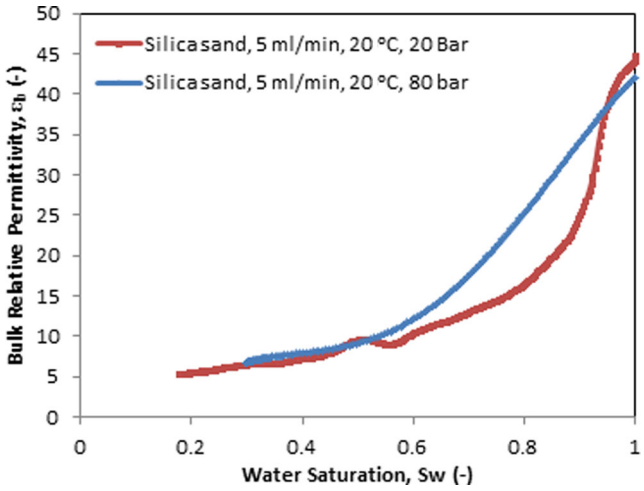

Figure 5. Effect of pressure on ε_b–S relationship in CO_2–water–silica sand system.

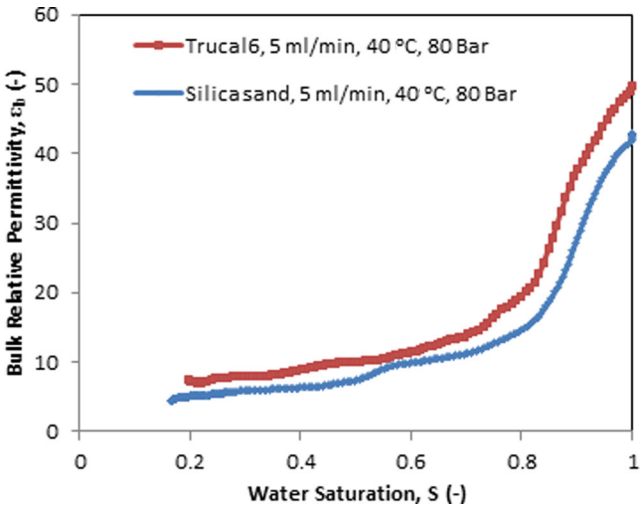

Figure 6. Effect of porous media samples on ε_b–S relationships in $scCO_2$–water–silica/limestone sand system.

From Figs 3 and 4, it can be seen that the ε_b–S relationship decreases as the water saturation reduces. This trend continues till a region of low water saturation where there is minimal change in the relationship as the water saturation reduces further. This was also shown in the work of Plug *et al.* (2007). This behaviour can be explained to be a result of reducing influence of water. Water has higher relative permittivity than the silica sand and the $scCO_2$ (Drnevich *et al.* 2001) and, thus seems to determine the overall trend of the ε_b–S curve as the displacement proceeds. Interestingly, the final value of the relative permittivity corresponds to what would be expected considering the bulk material present. For example, the silica sand has the relative permittivity value in the range 2.5–3.5 while that of the water is approximately 80 at ambient condition. At the start of the drainage when the influence of water is very high, ε_w of water dominates and the bulk relative permittivity starts at high value. Close to the end of the drainage, with minimal amount of water present in the bulk sand, one expects the property of sand to dominate with little amount of water present together with high saturation of CO_2 which is a resistive gas (Breen *et al.* 2012a). Thus, the bulk relative permittivity is slightly higher than the value of ε in dry silica sand owing to the traces of the water remaining.

3.1.1 *Effect of pressure*

Sequestration of CO_2 in saline aquifers takes place at different depths (Benson & Cole 2008). These correspond to different conditions of pressure and temperature. It is, therefore, important to understand the effect of pressure on the geoelectrical characteristics of $scCO_2$–water–sand system. In order to simulate these conditions in laboratory, we vary the injection pressures that correspond to varying injection depths.

Our investigation of the effect of pressure on the ε_b–S relationship for $scCO_2$–water–silica sand system shows that the ε_b increases as the pressure increases especially at higher water saturation ($S \geq$ 50 per cent). The finding is displayed in Fig. 5. The ε_b–S relationships at 20 and 80 bars have different profiles as water saturation reduces. ε_b values are higher at 80 bar than 20 bar for every comparable water saturation value. The difference remains conspicuous until around fifty percent saturation where the difference in the ε_b–S relationships for the two conditions becomes insignificant. We believe this behaviour has to do with the compressibility of the unconsolidated porous media (Sawabini *et al.* 1974) and the CO_2. Increasing pressure may increase the amount of soil-bound water as explained in the theory of soil-bound and bulk water by Wraith & Or (1999) and the results of Drnevich *et al.* (2001).

3.1.2 *Porous media effects*

Carbon sequestration is being carried out in many geological sites, especially those of carbonates and the silicates (Zhang *et al.* 2013; Lacinska *et al.* 2014). This makes it important to determine the effects of media sample characteristics on the ε_b–S relationship important. The effects of the carbonate and silicate media samples are shown in Fig. 6 for the Trucal 6 (limestone) and silica sand sample. It can be seen that the ε_b–S profile is generally higher in trucal 6 than the silica sand for the entire range of the water saturation. As shown in Table 1, the physical properties of the two sand samples are very similar but their chemical constituents are different. These chemical characteristics are expected to play more prominent role in the ε_b–S relationship for $scCO_2$-water system. Thus, the type of chemical properties of the porous media through which $scCO_2$-water system passes affects the ε_b–S relationship. According to Keller (1966), relative permittivity is a measure of the electrical polarization that takes place when an electric field. This might imply higher polarisation in the carbonate media with the presence of the electric field. As such, different profiles of ε_b–S relationship are expected as the strength of media and fluid polarity increases.

3.1.3 *Effect of temperature*

As stated before, carbon sequestration at different geological depths correspond to different conditions of temperature and pressure. Here, the impact of temperature on the ε_b–S relationship is also investigated. It was found that the ε_b–S profile decreases as the temperature increases in silica sand system. Fig. 7 shows the plots for the effect of temperature in silica sand. At 20 °C, the profile is highest for almost the entire water saturation range. Though, this is at subcritical state of CO_2 but the similar behaviour can be found in the supercritical state at 40 and 50 °C. The ε_b–S profile is higher at 40 °C than at 50 °C. Drnevich *et al.* (2001) reported similar behaviour in unconsolidated soil samples. They further show that the effect of temperature becomes more important at the temperature

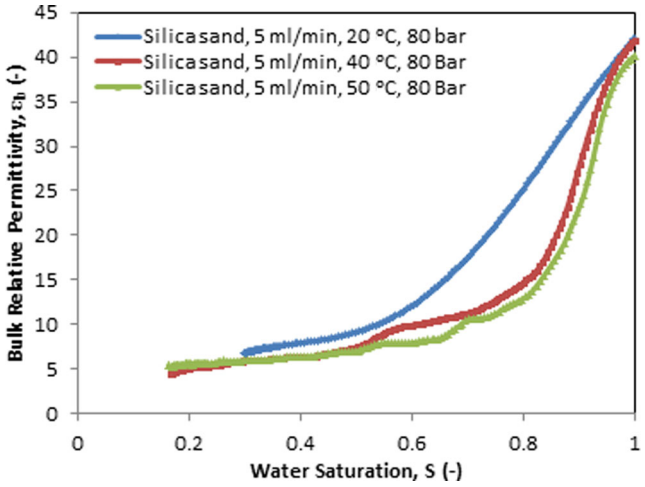

Figure 7. Effect of temperature on ε_b–S relationships in CO_2–water–silica sand system.

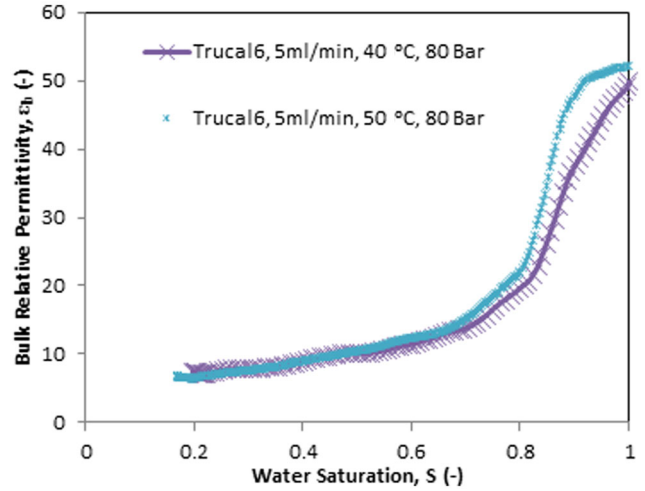

Figure 8. Effect of temperature on ε_b–S relationships at 80 bar in $scCO_2$–limestone (Trucal 6)–water system.

above 20 °C and can be ignored below this temperature. However, carbon sequestration is often carried out at temperature above 20 °C while possible leakage can follow different paths of various temperature and pressure conditions. Thus, the effect of temperature is essential for the geoelectrical monitoring techniques for the $scCO_2$-water system. This behaviour can be used to monitor change in aquifer conditions, especially when $scCO_2$ migrate in aquifer to regions of different temperature conditions. In the same way, the behaviour of ε_b–S relationships in the limestone exhibits similar patterns, but there is slight increase in the value of ε_b at higher temperature, especially at high water saturation. This is shown in Fig. 8. It can be seen that the ε_b–S profile at 50 °C is higher than at 40 °C, when the saturation is high. However, the difference becomes insignificant at lower water saturation. This can be attributed to the difference in the mineral solubility of the limestone under different temperature conditions. Coto *et al.* (2012) describes that the limestone becomes less soluble in water at higher temperature. This behaviour might influence surface stability of the mineral, which increases its relative permittivity at higher temperature. When an electric field is applied across a material, it is known that the electrostatic forces of the field influence the molecules of the material to rotate and align with the field. Though, there still exist motions

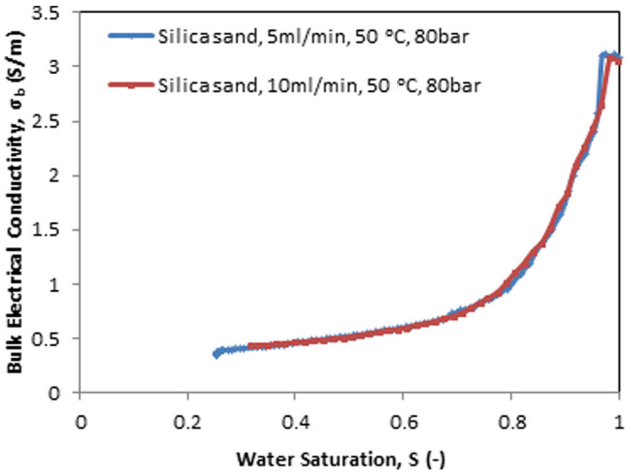

Figure 9. Effect of CO_2 injection rates on σ_b–S relationships in $scCO_2$–water–silica sand system (5 per cent NaCl).

among the molecules, upon increase in temperature, the average motion of the molecules increases which results in decreased alignment to the field and, hence, decreased ϵ. In silica sand, where the increased temperature results in higher dissolution (Rimstidt 1997), increased motion and less alignment to electrostatic field can be expected. Thus, there is decreased ε_b with increased temperature in silica sand at higher temperature. In the contrary, in the limestone, the increased temperature will lead to less dissolution. This may result in more alignment of the dipoles to the electrostatic field at higher temperature as a result of molecular stability in water–CO_2 system. However, this scenario calls for more investigations.

3.2 Electrical conductivity

Electrical conductivity, σ, is one of the fluid-fluid-media properties whose value is a function of water saturation (Keller 1966; Huang *et al.* 2005; Plug *et al.* 2007). It is important to know the factors influencing the σ_b–S relationships in porous media especially as relating to the geological carbon sequestration. Characterising the supercritical CO_2-water system with respect to these factors will enhance the prediction and understanding of the system especially in design of the monitoring procedures. As discussed before, the effect of CO_2 injection rate on the ε_b–S relationships in silica sand was tested and the result shown in Fig. 4. Fig. 9 is an illustration of σ_b–S relationships under different injection rates in silica sand. Though in Fig. 9, the relationship was examined under two different fast injection rates (5 and 10 ml min^{-1}), it is visible that there exists close similarity in the two σ_b–S profiles. Thus, it can be inferred that the ε_b–S and σ_b–S relationships are not affected by the desaturation rate in the unconsolidated sand unlike the P^c–S relationships. As such, dynamic effects are not found in the ε_b–S and σ_b–S relationships for $scCO_2$-brine/water. This is an important result in relation to the effective monitoring of the geological carbon sequestration as CO_2 migration can be reliably monitored using the same characterization function under dynamic displacement conditions, especially at the time close to the start of CO_2 injection prior to the attainment of equilibrium in the aquifer. Challenges of non-uniqueness in the two-phase flow characterization functions, especially P^c–S–K_r relationships, are of considerable concerns to researchers of two-phase flow systems in porous media (see e.g. Das *et al.* 2006; Joekar-Niasar & Hassanizadeh 2011; Khudaida & Das 2014; Abidoye *et al.* 2015).

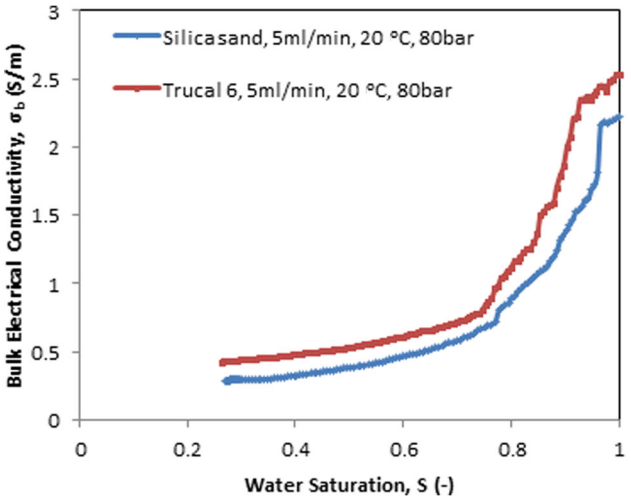

Figure 10. Effect of media sample types on σ_b–S relationships in CO_2–water–sand system at 5 per cent NaCl.

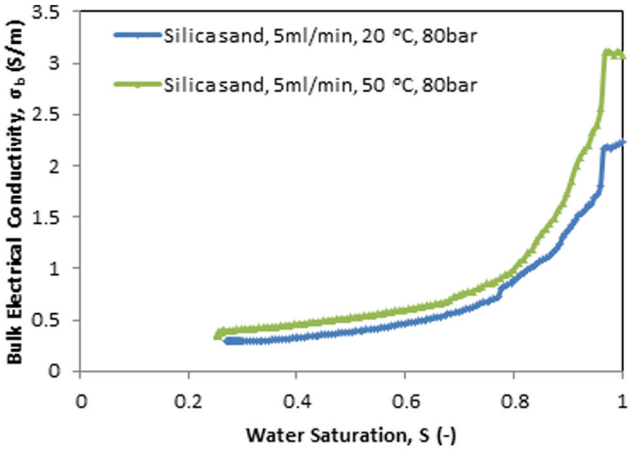

Figure 11. Effect of temperature on σ–S relationships in CO_2-brine system in silica sand at 5 per cent NaCl.

The influence of media sample type on σ_b–S curves is shown in Fig. 10 for the carbonate and silicate porous media. At all water saturation values, σ_b–S curve is higher in limestone (Trucal 6) than silica sand. This indicates that the conductivity of electric current is higher in the limestone. This can be attributed to the dissolution of the limestone in water thereby increasing the concentration of ions in the system. Carbonate rock is known for high dissolution rate (Plan 2005; Assayag *et al.* 2009).

Temperature also shows the impact on σ_b–S relationships as shown in Figs 11 and 12 for the CO_2 in silica sand and limestone, respectively. The σ_b–S curve increases as the temperature rises. This is more prominent at high water saturation. The trend in σ_b–S relationships appeared opposite to the effect of temperature in ε_b–S relationships in silica sand. For example, the ε_b–S curve decreases as the temperature increases while σ_b–S curve increases with temperature in silica sand. Also, it is interesting to see that the increase in σ_b–S curve with temperature is highest around 100 per cent water saturation and becomes less conspicuous as saturation decreases. This observation is similar to the report of Huang *et al.* (2005). They found that the electrical conductivity of the minerals in the earth's mantle depends strongly on water content but only weakly on temperature. The trends of ε_b–S and σ_b–S relationships are consistent

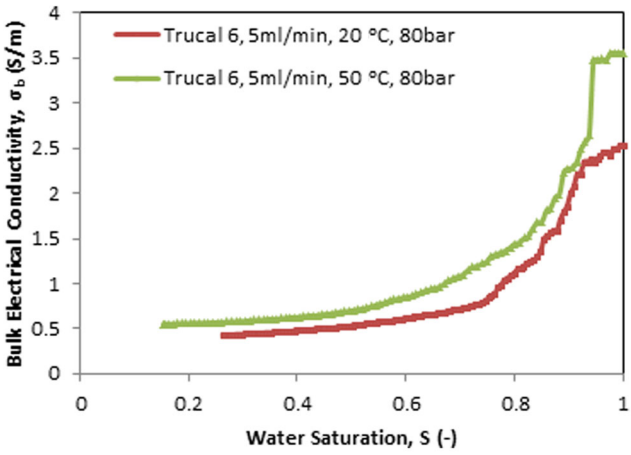

Figure 12. Effect of temperature on σ_b–S relationships in limestone (Trucal 6) (5 per cent NaCl).

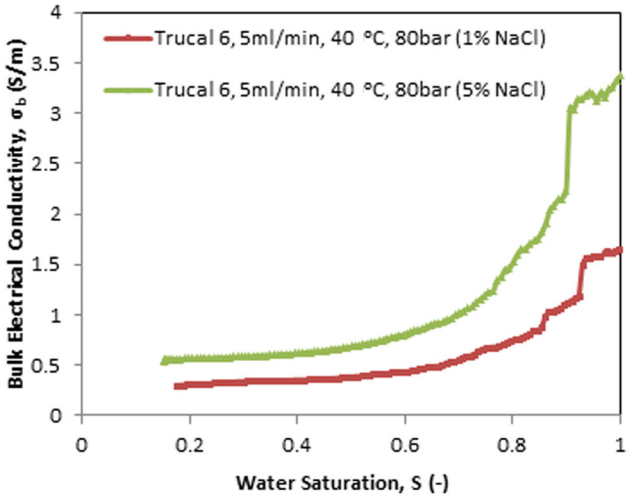

Figure 13. σ_b–S relationships at different salt concentrations at 40 °C in limestone (Trucal 6).

in the limestone with respect to temperature. Both show increments as the temperature increases.

3.3 Salt concentration

Saline aquifers in which carbon sequestrations take place may vary in the degree of salinity. Salinity can vary between 0.5 and 153 g l^{-1} in deep saline aquifers (Buttinelli *et al.* 2011). The effect of the variability of salinity is therefore examined on the σ_b–S relationship in this study. The σ_b–S relationships at different salt concentrations and temperatures in limestone (Trucal 6) are shown in Figs 13 and 14. As expected, σ_b–S curves increase with the increase in salt concentration and the gap increases with temperature. Since carbon sequestration takes place at geological sites of different salt concentrations, the results show that geoelectrical characteristics of the $scCO_2$–water system are site-specific.

3.4 Mathematical description of results

In this section, the results of the geoelectrical parameters for $scCO_2$-water/brine system are discussed with the aid of the petrophysical and mathematical relationships. It must be pointed out that the

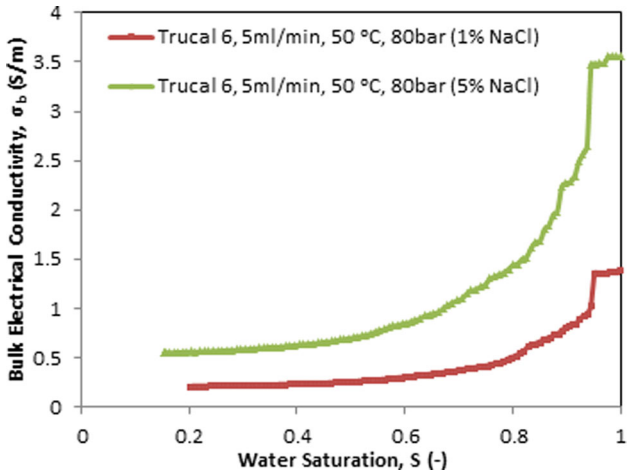

Figure 14. σ_b–S relationships at different salt concentrations at 50 °C in limestone (Trucal 6).

Table 3. Archie's (1942) exponents in different media.

Media sample	N	m
Silica sand	1.2	1.4
Limestone	1.5	1.2

experiments to determine the σ_b and ε_b were separately conducted. Archie's law (Archie 1942) was used to predict the σ_b in the silica sand and the limestone. The law is expressed as follows:

$$\sigma_b = \frac{S^n}{\phi^{-m}}\sigma_w \tag{2}$$

where S is the water saturation, σ_w is the pore water conductivity, ϕ denotes the connected porosity, n and m are the Archie's empirical parameters, which depend on the formation characteristics (Friedman 2005; Börner *et al.* 2013). The exponents in Archie's law were determined for each sample (silica sand or limestone). In order to solve for the exponents, eq. (2) was linearized using logarithm rules. The resulting linear equation was solved for the exponents ('m' and 'n') using MATLAB (Mathworks 2011). The exponents in the resulting models are shown in Table 3 for the silica sand and limestone.

Values of the exponents in Table 3 appeared to be in agreement with reports from literature. In loose sands and quartz, values in the range of 1.2–1.7 are reported for 'm' in the literature (see Archie 1942; Atkins & Smith 1961; Jackson *et al.* 1978). Also, values for 'n' in the literature are similar to that listed in the equations (see Vinegar & Waxman 1984; Hamamoto *et al.* 2010).

Furthermore, the results discussed in this work show that the ε_b is a function of many parameters, which include: water saturation (S), system temperature (T), pressure (P) and the initial value of ε_b (i). Initial value of ε_b refers to the value of ε_b for the porous medium with water before the injection of CO_2. This value of ε_b is important because it indicates the original state of water-filled porous medium, which eventually determines the ε_b–S profile. Thus, it can be written that,

$$\varepsilon_b = f(S, T, P, i) \tag{3}$$

The non-linear regression model in the XLSTAT (Microsoft 2014) was used to predict the observed ε_b values in this work. The non-linear regression model of polynomial degree 2 is shown in eq. (4):

$$\varepsilon_b = 213.86 - 47.17S - 0.074T + 0.048P - 9.18i + 72.71S^2 - 0.002T^2 + 0.11i^2 \tag{4}$$

The results of the prediction using eq. (4) are shown in Figs 15–17. Fig. 15 shows that the model captures the trend in the observed

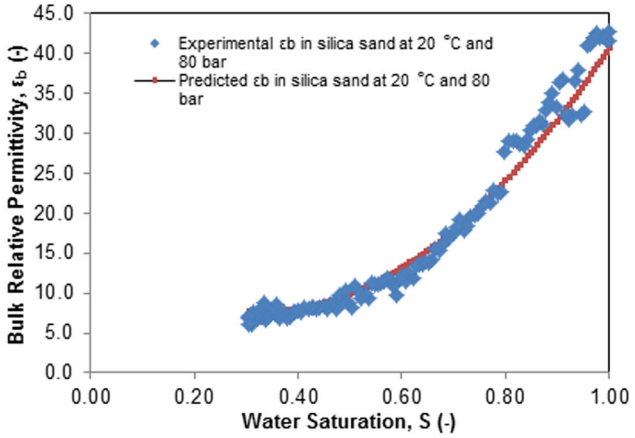

Figure 15. Prediction of the ε_b values in water–CO_2–silica sand system at 20 °C and 80 bar, using non-linear regression (RMSE = 2.70).

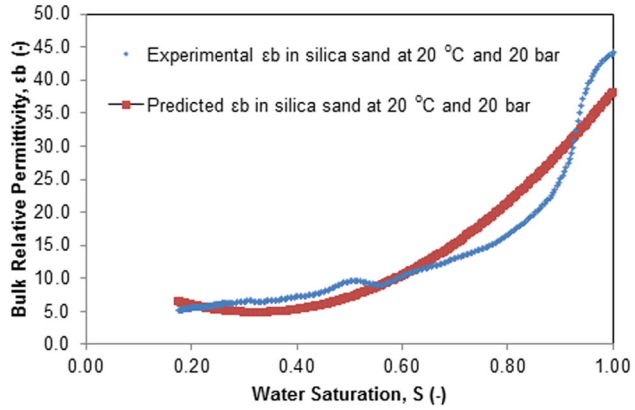

Figure 16. Prediction of the ε_b values in water–CO_2–silica sand system at 20 °C and 20 bar, using non-linear regression.

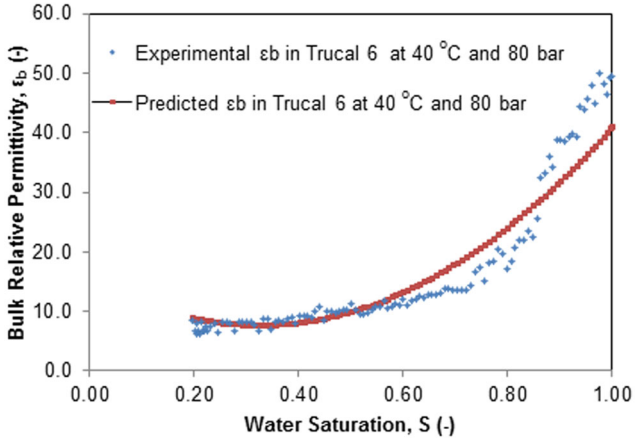

Figure 17. Prediction of the ε_b values in water–CO_2–limestone system at 40 °C and 80 bar using non-linear regression.

values of ε_b very well. The model shows reliability for wide range of water saturation. Also, in Figs 16 and 17, the model displays satisfactory performances for a range of saturation except at very low water saturation, where overfitting seems to occur. Around this low saturation region, the model displays slight increase in ε_b values with decreasing water saturation. But beyond this region (around $0 \leq S \leq 0.3$), the model gives good predictions of other range of water saturation. Thus, the non-linear regression presented in this work shows reliability in predicting the ε_b–S relationship for two-phase flow in porous media in wide saturation range.

Furthermore, a model presented by Roth *et al.* (1990) was explored in the prediction of the ε_b for $scCO_2$-water-porous media systems under different conditions. The objective of this model was to obtain a single calibration curve whose validity is not restricted to the experimental conditions, soil types or to a limited water content range. The model is expressed in eq. (5).

$$\varepsilon_b = (\theta\varepsilon_w^{\alpha} + (1-\phi)\varepsilon_s^{\alpha} + (\phi-\theta)\varepsilon_a^{\alpha})^{1/\alpha} \quad (5)$$

where ε_b is the composite or bulk relative permittivity for the system. ε_w, ε_s and ε_a represent the relative permittivities for the water, soil and CO_2, respectively. ϕ is the soil's porosity, $1-\phi$, θ and $\phi-\theta$ are the volume fractions for the soil, water and the CO_2, respectively. In the model, the constant parameter 'α' was described as crucial to the description of the composite dielectric number for different soils. Birchak *et al.* (1974), Alharthi & Lange (1987) as well as Roth *et al.* (1990) found the value of α as 0.5 to be very adequate in the mixing model. In this work, α value was determined from the experimental data presented above, by non-linear regression using XLSTAT (Microsoft 2014). From the regression analysis, α value of 0.8 was obtained with R^2 of 0.8 and RMSE of 5.4. Then, we compared the performances of the mixing model using the α value obtained by regression as well as the value recommended by the above-listed authors. Different temperatures involved in the data were taken into consideration. Temperature effects on the relative permittivities of silica sand and limestone were taken as negligible. But the temperature effects on the values of relative permittivities for water and CO_2 were taken into consideration. These assumptions were similar to those of Roth *et al.* (1990). Furthermore, the effect of pressure on the relative permittivity of CO_2 was considered using the publication of Michels & Michels (1933). Their publication considered the effect of temperature and pressure on relative permittivity of CO_2. Eq. (6) as expressed below was used to determine the relative permittivity for water at various temperatures.

$$\varepsilon_w = 78.54[1 - 4.579\times10^{-3}(T-25) + 1.19\times10^{-5}(T-25)^2 - 2.8\times10^{-8}(T-25)^3] \quad (6)$$

As said earlier, the performances of the model of Roth *et al.* were assessed with $\alpha = 0.5$ (Birchak *et al.* 1974; Alharthi & Lange 1987; Roth *et al.* 1990) as well as $\alpha = 0.8$, obtained from XLSTAT analysis. The results are shown in Figs 18 to 22. It can be seen in the figures that, at $\alpha = 0.5$, the mixing model shows reliability at lower water saturation, providing credible match of the experimental data for ε_b–S relationships. In most of the cases, the model provides reliable match of ε_b for more than 70 per cent of the corresponding saturation range. For example, it matches well the ε_b data in the water saturation range of 0–0.83 in the experiment conducted in silica sand at 20 °C and 20 bar. Similarly, ε_b data for water saturation range of 0–0.79 were well matched by the model in the experiment conducted in limestone (Trucal 6) at 40 °C and 80 bar. However, at this α value, the model deviates widely at higher water saturation. In comparison, α value of 0.8 seems to perform

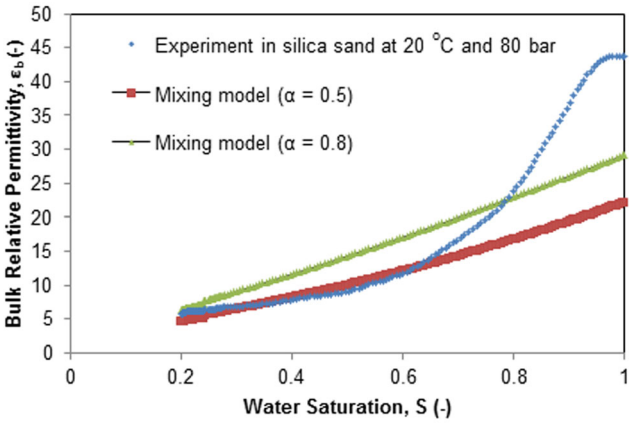

Figure 18. Performances of the mixing model (Roth *et al.* 1990) at different α values for prediction of experimental data in silica sand at 20 °C and 80 bar.

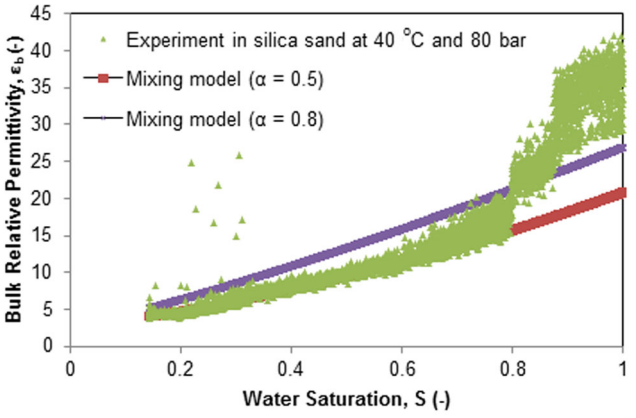

Figure 19. Performances of the mixing model (Roth *et al.* 1990) at different α values for prediction of experimental data in silica sand at 40 °C and 80 bar.

less satisfactorily. At this α value, the mixing model hardly matches the experimental data at both low and high water saturation. However, at α value of 0.8, the model appears to provide average values and linear relationship of the observed data. This behaviour can be seen in the Figs 18–22 where the model overpredicts the observed data at lower water saturation and underpredicts the data at higher

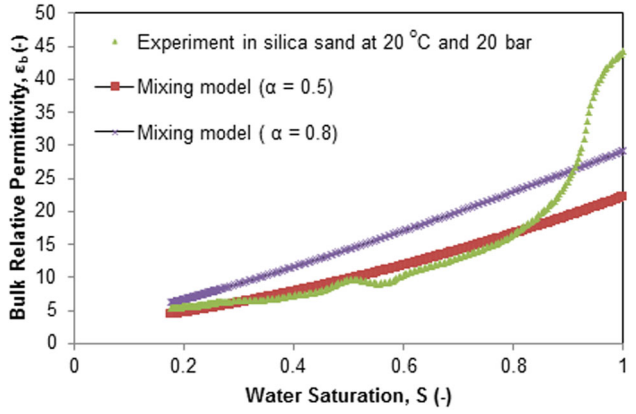

Figure 20. Performances of the mixing model (Roth *et al.* 1990) at different α values for prediction of experimental data in silica sand at 20 °C and 20 bar.

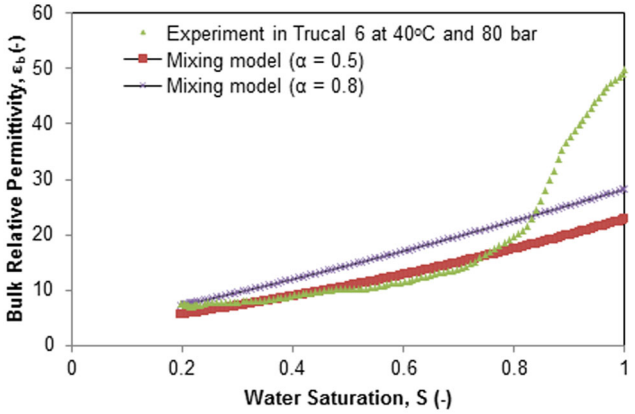

Figure 21. Performances of the mixing model (Roth *et al.* 1990) at different α values for prediction of experimental data in limestone at 40 °C and 80 bar.

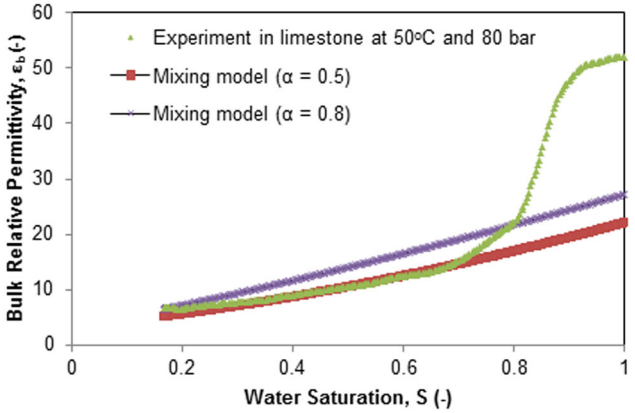

Figure 22. Performances of the mixing model (Roth *et al.* 1990) at different α values for prediction of experimental data in limestone at 50 °C and 80 bar.

saturation. The above effects of α values on the performances of the model Roth *et al.* (1990) corroborate their work, who found that the best fit value of the parameter α is 0.5. The limitation in the application of the model of Roth *et al.* (1990) may be attributed to the absence of the fluid pressure parameter. Effect of pressure on the relative permittivity of the CO_2 is well pointed out by Michels & Michels (1933). Its value changes with both temperature and pressure. Similarly, Wesch *et al.* (1996) show that the relative permittivity of CO_2 is highly dependent on pressure close to the critical pressure. The 2nd degree polynomial model developed in this work has the advantage of including the pressure parameter. Future effort will be geared towards its application and generalisation in wider range of water saturation using independent data.

4 CONCLUSIONS

The relative permittivity (ε_r) and the electrical conductivity (σ) are known to be functions of water saturation and the porous media samples. These relationships have been successfully investigated for the supercritical CO_2-brine/water system in both the carbonate (limestone) and silica sand samples. The bulk ε_r (ε_b) and σ (σ_b) values decrease as the water saturation decreases in the two porous media samples. While ε_b decreases with increase in temperature in silica sand, the trend in the limestone shows slight increase with temperature, especially at high water saturation. Also, the ε_b–S relationship is shown to be affected by the pressure in unconsolidated silica sand, which increases with the pressure of the domain. On the Contrary, the σ_b–S relationship increases as the temperature increases with more significance at higher water saturation in silica sand sample. Effects of porous media type on both the ε_b–S and σ_b–S curves shows that the relationships remain higher in the limestone than silica sand, under comparable conditions.

Based on the different injection rates investigated, there is no significant dynamic effect in ε_b–S and σ_b–S relationships for the supercritical CO_2–water system unlike capillary pressure-saturation-relative permeability (P^c–S–K_r) relationships. As such, geoelectrical characteristics are very reliable in the monitoring of supercritical CO_2-water system as found in geological carbon sequestration. It can be inferred from the results that the geoelectrical techniques are highly dependent on water saturation. This dependence is more conspicuous at higher water saturation. The polynomial fit developed in this work takes into consideration the pressure of the system as well as the initial bulk relative permittivity, prior to the injection of CO_2. The polynomial fit shows good reliability in the prediction of the geoelectrical properties of the CO_2–water–porous media system, especially at higher water saturation. In comparison, the mixing model from literature shows more reliability in the prediction of similar property at lower water saturation.

ACKNOWLEDGEMENTS

A PhD studentship awarded to Mr Luqman Abidoye under the Petroleum Technology Development Fund (PTDF), Nigeria, to carry out the work in this paper is much appreciated. Support from the Technical Support team at Department of Chemical Engineering, Loughborough University, UK, is gratefully acknowledged. The comments of the two anonymous referees, which have helped to improve the paper significantly, are gratefully acknowledged.

REFERENCES

Abidoye, L.K., Das, D.B. & Khudaida, K., 2015. Geological carbon sequestration in the context of two-phase flow in porous media: a review, *J. Crit. Rev. Environ. Sci. Technol.,* **45**(11), 1105–1147.

Aggelopoulos, C.A. & Tsakiroglou, C.D., 2008. The effect of micro-heterogeneity and capillary number on capillary pressure and relative permeability curves of soils, *Geoderma,* **148**(1), 25–34.

Alharthi, A. & Lange, J., 1987. Soil water saturation: dielectric determination, *Water Resour. Res.,* **23**(4), 591–595.

Archie, G., 1942. The electrical resistivity log as an aid in determining some reservoir characteristics, *Trans. Am. Inst. Mining Metallur. Eng.,* **146,** 54–61.

Assayag, N., Matter, J., Ader, M., Goldberg, D. & Agrinier, P., 2009. Water–rock interactions during a CO_2 injection field-test: implications on host rock dissolution and alteration effects, *Chem. Geol.,* **265**(1), 227–235.

Atkins, E.R. & Smith, G.H., 1961. The significance of particle shape in formation factor-porosity relationships, *Petrol. Tech.,* **13,** 285–291.

Benson, S.M. & Cole, D.R., 2008. CO_2 sequestration in deep sedimentary formations, *Elements,* **4**(5), 325–331.

Birchak, J.R., Gardner, C.G., Hip, J.E. & Victor, J.M., 1974. High dielectric constant microwave probes for sensing soil moisture, *Proc. IEEE,* **62**(1), 93–98.

Börner, J.H., Herdegen, V., Repke, J.U. & Spitzer, K., 2013. The impact of CO_2 on the electrical properties of water bearing porous media–laboratory experiments with respect to carbon capture and storage, *Geophys. Prospect.,* **61**(s1), 446–460.

Breen, S.J., Carrigan, C.R., LaBrecque, D.J. & Detwiler, R.L., 2012. Bench-scale experiments to evaluate electrical resistivity tomography as a

monitoring tool for geologic CO_2 sequestration, *Int. J. Greenhouse Gas Contl.,* **9,** 484–494.

Buttinelli, M., Procesi, M., Cantucci, B., Quattrocchi, F. & Boschi, E., 2011. The geo-database of caprock quality and deep saline aquifers distribution for geological storage of CO_2 in Italy, *Energy,* **36**(5), 2968–2983.

Camps-Roach, G., O'Carroll, D.M., Newson, T.A., Sakaki, T. & Illangasekare, T.H., 2010. Experimental investigation of dynamic effects in capillary pressure: grain size dependency and upscaling, *Water Resour. Res.,* **46**(8), W08544, doi:10.1029/2009WR008881.

Coto, B., Martos, C., Peña, J.L., Rodríguez, R. & Pastor, G., 2012. Effects in the solubility of $CaCO_3$: experimental study and model description, *Fluid Phase Equilibria,* **324,** 1–7.

Das, D.B. & Mirzaei, M., 2013. Experimental measurement of dynamic effect in capillary pressure relationship for two-phase flow in weakly layered porous media, *AIChE J.,* **59**(5), 1723–1734.

Das, D.B., Mirzaei, M. & Widdows, N., 2006. Non-uniqueness in capillary pressure–saturation–relative permeability relationships for two-phase flow in porous media: interplay between intensity and distribution of random micro-heterogeneities, *Chem. Eng. Sci.,* **61**(20), 6786–6803.

Das, D.B., Gauldie, R. & Mirzaei, M., 2007. Dynamic effects for two-phase flow in porous media: fluid property effects, *AIChE J.,* **53**(10), 2505–2520.

Das, D.B., Gill, B.S., Abidoye, L.K. & Khudaida, K. 2014. Numerical simulation of dynamic effect in capillary pressure-saturation relationship for supercritical carbon dioxide-water flow in porous domain, *AIChE J.,* **60**(12), 4266–4278.

Dethlefsen, F., Köber, R., Schäfer, D., Hagrey, S.A.A., Hornbruch, G., Ebert, M. & Dahmke, A., 2013. Monitoring approaches for detecting and evaluating CO_2 and formation water leakages into near-surface aquifers, *Ener. Proc.,* **37,** 4886–4893.

Doughty, C., 2007. Modeling geologic storage of carbon dioxide: comparison of non-hysteretic and hysteretic characteristic curves, *Ener. Conver. Manag.,* **48**(6), 1768–1781.

Doussan, C. & Ruy, S., 2009. Prediction of unsaturated soil hydraulic conductivity with electrical conductivity, *Water Resour. Res.,* **45**(10), doi:10.1029/2008WR007309.

Drnevich, V.P., Lovell, J., Tishmack, J., Yu, X. & Zhang, J., 2001. *Temperature Effects on Dielectric Constant Determined by Time Domain Reflectometry, TDR 2001: Innovative Applications of TDR Technology,* Infrastructure Technology Institute, Northwestern University, Evanston, IL, September.

Ellis, M.H., Sinha, M.C., Minshull, T.A., Sothcott, J. & Best, A.I., 2010. An anisotropic model for the electrical resistivity of two-phase geologic materials, *Geophysics,* **75**(6), E161–E170.

Friedman, S.P., 2005. Soil properties influencing apparent electrical conductivity: a review, *Comput. Electr. Agric.,* **46**(1), 45–70.

Goel, G. & O'Carroll, D.M., 2011. Experimental investigation of nonequilibrium capillarity effects: fluid viscosity effects, *Water Resour. Res.,* **47**(9), W09507, doi:10.1029/2010WR009861.

Hamamoto, S., Moldrup, P., Kawamoto, K. & Komatsu, T., 2010. Excluded-volume expansion of Archie's law for gas and solute diffusivities and electrical and thermal conductivities in variably saturated porous media, *Water Resour. Res.,* **46**(6), doi:10.1029/2009WR008424.

Hassanizadeh, S.M., Celia, M.A. & Dahle, H.K., 2002. Dynamic effect in the capillary pressure–saturation relationship and its impacts on unsaturated flow, *Vadose Zone J.,* **1**(1), 38–57.

Hou, L., Chen, L. & Kibbey, T.C.G., 2012. Dynamic capillary effects in a small-volume unsaturated porous medium: implications of sensor response and gas pressure gradients for understanding system dependencies, *Water Resour. Res.,* **48**(11), W11522, doi:10.1029/2012WR012434.

Huang, X., Xu, Y. & Karato, S., 2005. Water content in the transition zone from electrical conductivity of wadsleyite and ringwoodite, *Nature,* **434**(7034), 746–749.

Jackson, P.D., Smith, D.T. & Stanford, P.N., 1978. Resistivity-porosity-particle shape relationships for marine sands, *Geophysics,* **43**(6), 1250–1268.

Joekar-Niasar, V. & Majid Hassanizadeh, S., 2011. Effect of fluids properties on non-equilibrium capillarity effects: dynamic pore-network modeling, *Int. J. Multiphase Flow,* **37**(2), 198–214.

Kalaydjian, F., 1992. Effect of the flow rate on an imbibtion capillary pressure curve-theory versus experiment, in *Proceedings of the SCA European Core Analysis Symposium,* Paris, France.

Keller, G.V., 1966. Section 26: electrical properties of rocks and minerals, *Geol. Soc. Am. Mem.,* **97,** 553–577.

Khudaida, K. & Das, D.B., 2014. A numerical study of capillary pressure-saturation relationship for supercritical carbon dioxide (CO_2) injection in deep saline aquifer, *Chem. Eng. Res. Des.,* **92**(12), 3017–3030.

Knight, R., 1991. Hysteresis in the electrical resistivity of partially saturated sandstones, *Geophysics,* **56**(12), 2139–2147.

Knight, R. & Abad, A., 1995. Rock/water interaction in dielectric properties: experiments with hydrophobic sandstones, *Geophysics,* **60**(2), 431–436.

Knight, R.J. & Nur, A., 1987. The dielectric constant of sandstones, 60 kHz to 4 MHz, *Geophysics,* **52**(5), 644–654.

Lacinska, A.M., Styles, M.T. & Farrant, A.R., 2014. Near-surface diagenesis of ophiolite-derived conglomerates of the Barzaman Formation, United Arab Emirates: a natural analogue for permanent CO_2 sequestration via mineral carbonation of ultramafic rocks, *Geol. Soc. Lond., Spec. Publ.,* **392**(1), 343–360.

Lagneau, V., Pipart, A. & Catalette, H., 2005. Reactive Transport modelling and long term behaviour of CO_2 Sequestration in Saline Aquifers, *Oil Gas Sci. Technol.,* **60**(2), 231–247.

Longeron, D.G., Argaud, M.J. & Feraud, J.P., 1989. Effect of overburden pressure and the nature and microscopic distribution of fluids on electrical properties of rock samples, *SPE Format. Eval.,* **4**(02), 194–202.

Mahmood, A., Warsi, M.F., Ashiq, M.N. & Sher, M., 2012. Improvements in electrical and dielectric properties of substituted multiferroic $LaMnO_3$ based nanostructures synthesized by co-precipitation method, *Mater. Res. Bull.,* **47**(12), 4197–4202.

Michels, A. & Michels, C., 1933. *Philosophical Transactions of the Royal Society of London. Series A, Containing Papers of a Mathematical or Physical Character,* Vol. 231, The Royal Society, pp. 409–434.

Mirzaei, M. & Das, D.B., 2013. Experimental investigation of hysteretic dynamic effect in capillary pressure-saturation relationship for two-phase flow in porous media, *AIChE J.,* **59**(10), 3958–3974.

Nakatsuka, Y., Xue, Z., Garcia, H. & Matsuoka, T., 2010. Experimental study on CO_2 monitoring and quantification of stored CO_2 in saline formations using resistivity measurements, *Int. J. Greenhouse Gas Contl.,* **4**(2), 209–216.

Nguyen, B.-L., Bruining, J. & Slob, E.C., 1999. Effects of wettability on dielectric properties of porous media, in *Proceedings of the SPE Annual Technical Conference,* pp. 153–160.

Plan, L., 2005. Factors controlling carbonate dissolution rates quantified in a field test in the Austrian alps, *Geomorphology,* **68**(3), 201–212.

Plug, W.-J. & Bruining, J., 2007. Capillary pressure for the sand–CO_2–water system under various pressure conditions. Application to CO_2 sequestration, *Adv. Water Resour.,* **30**(11), 2339–2353.

Plug, W.J., Moreno, L.M., Bruining, J. & Slob, E.C., 2007. Simultaneous measurement of capillary pressure and dielectric constant in porous media, *PIERS Online,* **3**(4), 549–553.

Power, C., Gerhard, J.I., Tsourlos, P. & Giannopoulos, A., 2013. A new coupled model for simulating the mapping of dense nonaqueous phase liquids using electrical resistivity tomography, *Geophysics,* **78**(4), EN1–EN15.

Revil, A., Cathles, L., Losh, S. & Nunn, J., 1998. Electrical conductivity in shaly sands with geophysical applications, *J. geophys. Res.: Solid Earth,* **103,** 23–23.

Rimstidt, J.D., 1997. Quartz solubility at low temperatures, *Geochim. Cosmochim. Acta,* **61**(13), 2553–2558.

Robinson, D.A., Gardner, C.M.K. & Cooper, J.D., 1999. Measurement of relative permittivity in sandy soils using TDR, capacitance and theta probes: comparison, including the effects of bulk soil electrical conductivity, *J. Hydrol.,* **223**(3), 198–211.

Roth, K., Schulin, R., Flühler, H. & Attinger, W., 1990. Calibration of time domain reflectometry for water content measurement using a composite dielectric approach, *Water Resour. Res.,* **26**(10), 2267–2273.

Sawabini, C.T., Chilingar, G.V. & Allen, B.R., 1974. Compressibility of unconsolidated, arkosic oil sands: 11F, 31R Soc. Petroleum engrs. J. V14, N2, Apr. 1974, P132–139, *Int. J. Rock Mech. Mining Sci. Geomech. Abstr.,* 201.

Schmutz, M., Blondel, A. & Revil, A., 2012. Saturation dependence of the quadrature conductivity of oil-bearing sands, *Geophys. Res. Lett.,* **39**(3), L03402, doi:10.1029/2011GL050474.

Solymar, L., Walsh, D. & Syms, R.R.A., 2014. *Electrical Properties of Materials,* Oxford Univ. Press.

Verwer, K., Eberli, G.P. & Weger, R.J., 2011. Effect of pore structure on electrical resistivity in carbonates, *AAPG Bull.,* **95**(2), 175–190.

Vinegar, H.J. & Waxman, M.H., 1984. Induced polarization of shaly sands, *Geophysics,* **49**(8), 1267–1287.

Wesch, A., Dahmen, N. & Ebert, K.H., 1996. Measuring the static dielectric constants of pure carbon dioxide and carbon dioxide mixed with ethanol and toluene at elevated pressures, *Berichte der Bunsengesellschaft für physikalische Chemie,* **100**(8), 1368–1371.

Wraith, J.M. & Or, D., 1999. Temperature effects on soil bulk dielectric permittivity measured by time domain reflectometry: experimental evidence and hypothesis development, *Water Resour. Res.,* **35**(2), 361–369.

Zhang, Y.Q., Radha, A.V. & Navrotsky, A., 2013. Thermochemistry of two calcium silicate carbonate minerals: scawtite, Ca7 $(Si_6O_{18})(CO_3) \bullet 2H_2O$, and spurrite, $Ca_5\ (SiO_4)_2\ (CO_3)$, *Geochim. Cosmochim. Acta,* **115,** 92–99.